

A Bidirectional Fabric-based Pneumatic Actuator for the Infant Shoulder: Design and Comparative Kinematic Analysis

Ipsita Sahin,¹ Jared Dube,¹ Caio Mucchiani,² Konstantinos Karydis,² and Elena Kokkoni¹

Abstract—This paper presents the design and assessment of a fabric-based soft pneumatic actuator with low pressurization requirements for actuation making it suitable for upper extremity assistive devices for infants. The goal is to support shoulder abduction and adduction without prohibiting motion in other planes or obstructing elbow joint motion. First, the performance of a family of actuator designs with internal air cells is explored via simulation. The actuators are parameterized by the number of cells and their width. Physically viable actuator variants identified through the simulation are further tested via hardware experiments. Two designs are selected and tested on a custom-built physical model based on an infant's body anthropometrics. Comparisons between force exerted to lift the arm, movement smoothness, path length and maximum shoulder angle reached inform which design is better suited for its use as an actuator for pediatric wearable assistive devices, along with other insights for future work.

I. INTRODUCTION

Though typically developing infants move their arms and explore their environment from the first months of age, infants with or at risk for upper extremity (UE) impairments show delayed emergence of UE motor milestones, and/or diminished ability to perform motor actions [1]. Providing infants with opportunities for training through the use of assistive devices can lead to improvements on their motor function [2]. Currently, UE assistive devices for infants are limited [3] and are mainly passive (notable examples are the Pediatric Wilmington Robotic Exoskeleton, a rigid 3D-printed, two-link device [4]; and, PlaySkin Lift, a soft wearable with mechanical inserts [5]). Actuated devices, however, can deliver targeted and on-demand assistive forces that could directly adapt to the user as they grow and their abilities change [6] (e.g., compared to the need for manual adjustment of mechanical assistance, as seen in [4], [5]). Our recent work on the development of an actuated UE wearable device for infants has utilized silicone-based pneumatically-controlled actuators to provide assistance at both elbow and shoulder joints [7]. The current paper extends this work by introducing new soft actuator designs for the shoulder joint.

Soft materials and compliant structures are increasingly being used for actuation in assistive and rehabilitation devices [8]–[13]. To be functional and practical, soft robotic actuators need to meet certain design specifications, such

as high power density, accuracy and repeatability in both manufacturing and performance [14]–[17]. Soft pneumatic actuators are lightweight, have simpler control specifications, and provide inherent safety (i.e. low risk of getting injured in case of malfunction) over other complex engineered devices [18]. Commonly used soft pneumatic actuators are Elastic Inflatable Actuators (EIAs), which include silicone-based EIAs and fabric-based EIAs, among others.

EIAs are powered by pressurized gas (or liquid) and are capable of achieving large strokes with very little friction, thus exhibiting distributed force generation [19]. Compared to silicone-based EIAs, fabric-based EIAs require lower pressure because of the non-extensibility of the fabric material. Also, fabric-based EIAs can be built faster and at a lower overall cost than silicone-based ones. Fabrication of the latter involves several steps that may take hours to complete: 3D printing molds for different parts (e.g., ~ 1.5 hrs [20], etc.), multi-staged casting and curing of silicone (e.g., 0.5-16 hrs for DragonSkin, etc.), and assembling parts using suitable adhesives. On the other hand, fabric-based soft pneumatic actuators, such as those made of flexible Thermoplastic PolyUrethane (TPU) coated nylon fabric, can be built fast, in a cost-effective manner, and without the use of any specialized equipment [21]. Even fabric-based actuators with complicated designs (e.g., use of pleats on the actuator to guide motion during inflation [22], application of double-layered inner bladders to prevent air-leakage [23], fabrication of wrinkle actuators using specialized equipment like high-frequency electromagnetic welding [24], etc.) that do require significant fabrication time, may still be made faster than their silicone counterparts with similar functionality.

Fabric-based shoulder actuators are seen in UE devices intended for use by adults [25], [26], and children [27] but not infants (exception is [28] which contains underarm actuators for the purpose of assisting postural transitions from lying to sitting). In this work, we explored the use of fabric-based EIAs as an alternative to the silicon-based EIAs previously used for our application [7].

II. FABRICATION PROCESS, DESIGN CONSIDERATIONS, AND PRELIMINARY FEASIBILITY IN SIMULATION

A new family of flexible TPU fabric-based, multi-pouched actuators for shoulder abduction/adduction is presented. Initially, first-principles-based numerical simulation was conducted to determine the preliminary feasibility of all proposed actuator variants prior to physical testing. Down-selected actuator variants were then fabricated and tested on a custom-built physical infant model.

¹Dept. of Bioengineering; ²Dept. of Electrical and Computer Engineering, University of California, Riverside, 900 University Ave, Riverside, CA 92521, USA. Email:{isahi001, jdube004, caiocesr, karydis, elenak}@ucr.edu. We gratefully acknowledge the support of NSF # CMMI-2133084. Any opinions, findings, and conclusions or recommendations expressed in this material are those of the authors and do not necessarily reflect the views of NSF.

A. Design Approach

The design of our proposed fabric-based actuators with air pouches (cells) (Fig. 1) improves upon the design of the silicone-based shoulder actuators in [7]. The new actuators are low-profile (i.e. non-obtrusive when not inflated) and can be fabricated fast (<20 min). We use flexible and lightweight fabric (Oxford 200D heat-sealable coated fabric [properties listed in Table I]). The fabric can be heat-sealed via non-specialized equipment like a household iron. To reduce areas that may become potential leakage points, we cut strips of fabric, wrap them around, and seal together the two opposite coated sides (instead of cutting two separate pieces and seal them at their periphery). This can constrain potential leakage to the point where tubing is embedded into a cell.

TABLE I
NYLON-OXFORD FABRIC PROPERTIES

Elastic Modulus (N/m^2)	498000000
Poisson's Ratio (N/A)	0.35
Shear Modulus (N/m^2)	184400000
Mass Density (kg/m^3)	757.58
Tensile Strength (N/m^2)	17520
Compressive Strength (N/m^2)	103421000
Yield Strength (N/m^2)	58605000
Thermal Expansion Coefficient ($1/K$)	1.00E-06
Thermal Conductivity ($W/(m - K)$)	0.53
Specific Heat ($J/(kg - K)$)	1386

We focused on the design of rectangular actuators (Fig. 1). The actuators contain non-inflatable and inflatable portions, and are parameterized based on three characteristics: i) their total length (kept herein constant at 254 mm), ii) their width (we consider five cases of 50.8 mm, 44.45 mm, 38.1 mm, 31.75 mm and 25.4 mm), and iii) the number of discrete cells the inflatable part is divided into (1 – 4 cells). The non-inflatable portion contains two 50.8 mm-long areas at each side, used for attaching the actuators onto the body. The inflatable portion is the area in the middle and measures 152.4 mm in length. Table II contains the 20 distinct actuator variants considered in this work.¹ Their main dimensions (importantly length and width) were informed by anthropometric data of the infant population reported in the literature. The upper arm length for male and female infants of 6-24 months of age varies on average between 142 – 188 mm and 135 – 183 mm, respectively [29].

Our proposed fabric-based actuators are lightweight, making them ideal for use in pediatric assistive and rehabilitation devices. Specifically, their weight varies between 3.8 g for thinner ones and 8.2 g for wider ones, which is a reduction of over 84% compared to the silicone-based ones [7] that weigh about 51.2 g each. Lightweight actuators result in smaller inertia and hence lower contact force and lower overall momentum, which is critical for safety.

¹This type of design can directly scale up to create larger actuators, e.g., targeted to older children. However, scaling down is determined by the available fabrication means to heat-seal the fabric (smaller actuators require thinner heat-sealed seams which may be achieved e.g., by low-heat precision-tip ironing) as well as its practical utility given the application context. For instance, as discussed later, actuators with more than four cells do not generate enough force required for the present application.

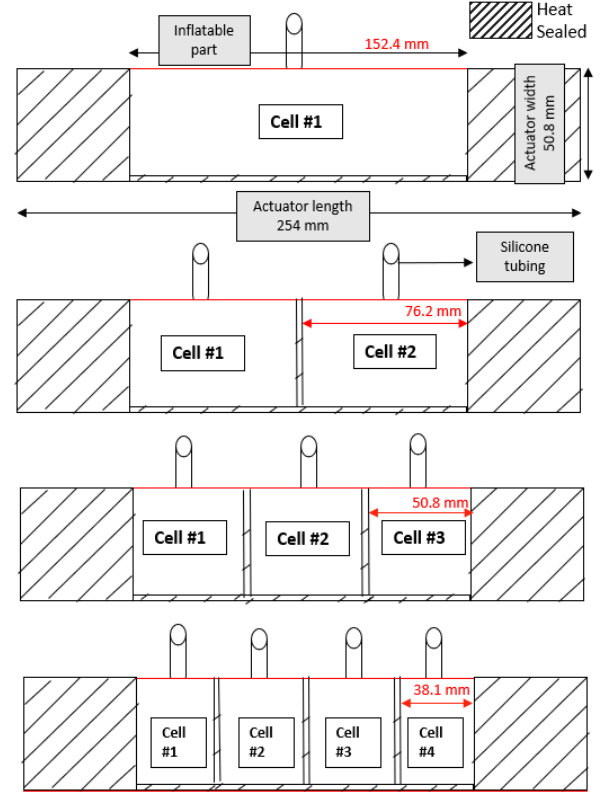


Fig. 1. Cross-section view of the proposed family of parameterized soft fabric-based pneumatic actuators considered in this work.

TABLE II
KEY ACTUATOR DESIGN PARAMETERS

Types	Cell Length (mm)	Total length (mm)	Width (5 cases)
1 Cell	152.40	254	\mathcal{W}
2 Cell	76.20	254	\mathcal{W}
3 Cell	50.80	254	\mathcal{W}
4 Cell	38.10	254	\mathcal{W}

* where $\mathcal{W} = \{50.80, 44.45, 38.10, 31.75, 25.40\}$ mm

B. Feasibility Assessment in Simulation

The performance and design feasibility of the proposed family of actuator designs (Table II) was first assessed through simulated experiments (SolidWorks; Dassault Systems, Waltham, MA). Simulations were used to estimate the stress, strain, deformation scale, and displacement, to identify actuator designs that can maximize the force output to be useful for arm abduction without failing. Simulated experiments serve as the basis to guide hardware development in the sense of filtering out some of the parametrization listed in Table II that are not expected to be physically viable.

Simulations used the TPU-coated nylon from the software's material library with yield strength of $5.86e^7 N/m^2$. All components of the simulated actuators employed the shelling function on 10 mm thick cells to create 9 mm pockets within all the given actuators cells, which closely matches the height of the physical actuators. An outward pressure from within the cells against their inner surfaces was applied to find the maximum pressure up to which the actuators avoid functional failure.

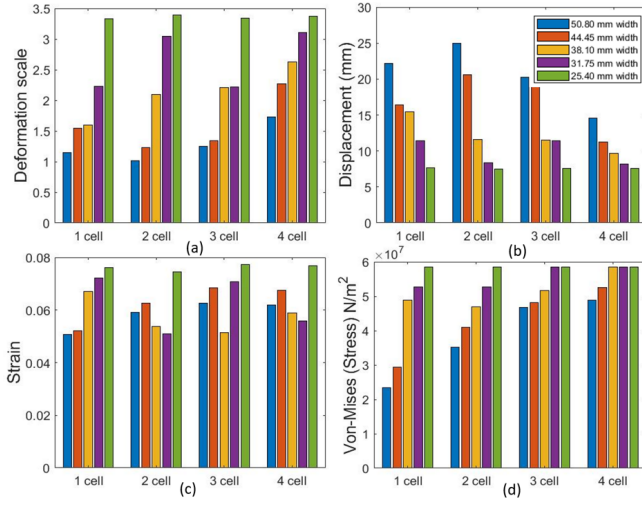


Fig. 2. Effects of decreasing width for all 20 actuators. Deformation scale, strain and stress increase but displacement decreases with smaller widths.

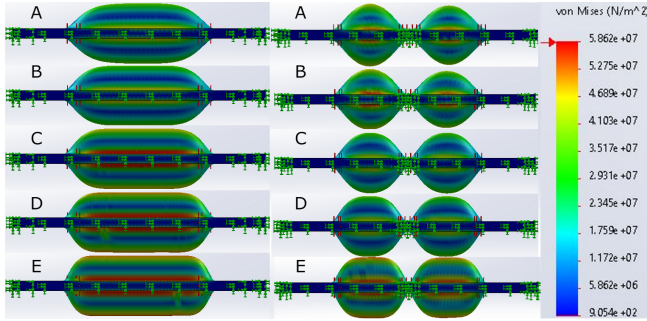


Fig. 3. Simulation for the shoulder actuators for various geometries i.e. decreasing the width from A (50.80mm) to E (38.10mm) (*top – bottom*) of Von Mises stress contour plots for stresses in 1 cell (*left*) and 2 cell (*right*). As the width decreases, the von Mises value increases.

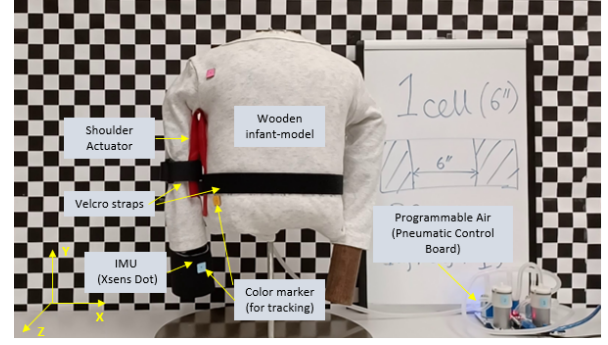
It can be seen in Fig. 2 the cell width is directly proportional to the amount of displacement, whereas the deformation scale and strain are inversely proportional. Furthermore, a decrease in cell width (from 50.8 mm to 25.4 mm) causes a critical error as von Mises values exceed the yield strength and strain is much higher (Fig. 3). To determine the optimal number of cells, note the increasing trend among number of cells, von Mises and strain. This suggests that actuators with fewer cells and higher width are expected to perform better.

Armed with this analysis, 1- and 2-cell actuators of the highest width (50.80 mm) were deemed to be most viable choices for shoulder abduction/adduction with lower chances of failure, and hence were also tested experimentally.

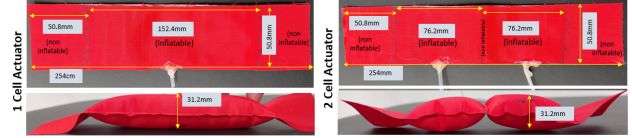
III. EXPERIMENTAL TESTING AND EVALUATION

A. Experimental Setup

Inflation and deflation of the actuators were controlled using an off-body pneumatic control board (Programmable-Air—an open-source hardware kit to control inflatable soft robots). The board has two compressor/vacuum pumps and three pneumatic valves to control the airflow during inflation and deflation and weighs 0.35 kg (Fig. 4a). The pumps have a flow rate of 2 lit/min. The Pulse Width Modulation (PWM) or the duty cycle of the pump can be varied from 0% to 100%, and although the pump may turn on around



(a) The experimental setup with the actuator placed under the arm.

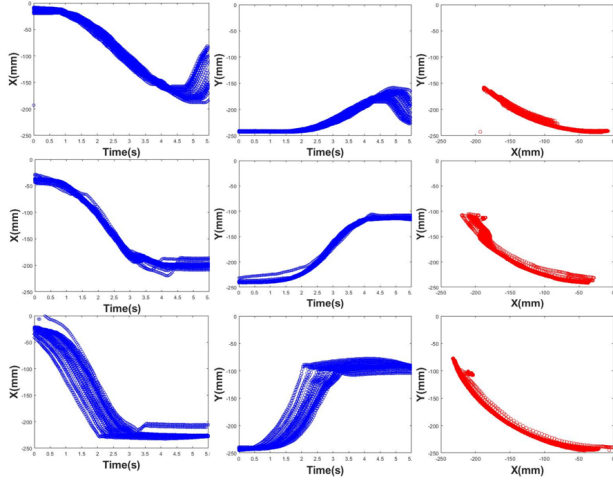


(b) 1-cell (left) and 2-cell (right) physical actuator prototypes at deflated state (top) and at full inflation (bottom).

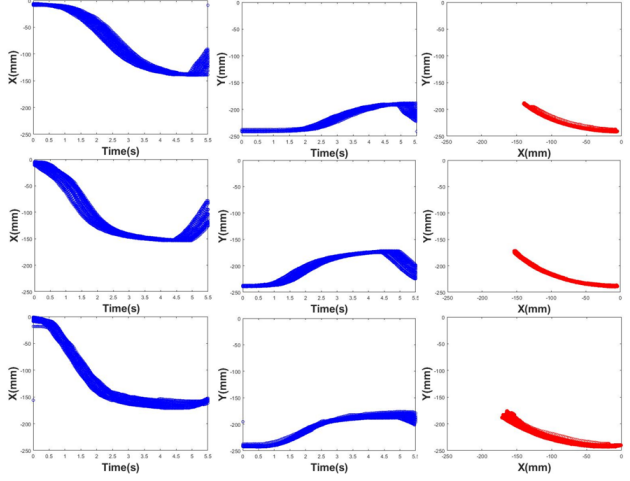
Fig. 4. Physical experimentation setup and sample actuator prototypes. 20% duty cycle, the lower the % duty cycle, the longer it will take to inflate/deflate. The board can create pressure varying between $[-7.5, +7.5]$ psi. An Arduino Nano (AT-Mega328P) connects the board to a computer via microUSB. This electro-pneumatics board is powered up using a 12V adapter. The board also has a pressure sensor (SMPP-03). After full inflation, if a certain internal pressure is reached, airflow automatically stops to prevent leakage and/or actuator damage.

For the physical experiments, the two down-selected actuator variants (1-cell and 2-cell actuators; Fig. 4b) were placed on a physical model scaled approximately to the 50th percentile of a 12-month-old infant's upper body [29] using velcro straps on the non-inflatable portions (Fig. 4a). The arm was linked to the torso through a 3-DOF ball-and-socket shoulder joint. Actuator placement was selected such that it can support shoulder abduction/adduction without hindering rotation about the other axes. In the experiments, different conditions were considered by varying i) the duty cycle of the pneumatic control board (50%, 75% and 100%), and ii) the inflation/deflation times ([1–5] sec in 1 sec increments). Both actuators went through 30 trials of abduction and adduction for each condition. Video recordings from the experiments were used to extract the 2D position of the end-effector (indicated by a color marker Fig. 4(a)) of the arm (www.kinovea.org; v0.9.5). An Inertial Measurement Unit (IMU) (Xsens DOT; Xsens Technologies B.V., Enschede, The Netherlands) was placed at the end-effector to collect kinematic data (Euler angles, acceleration and velocity) at a sampling rate of 60 Hz. Lastly, the force exerted by the arm was measured with the actuator powered on, using a four-wire load cell and HX711 amplifier.

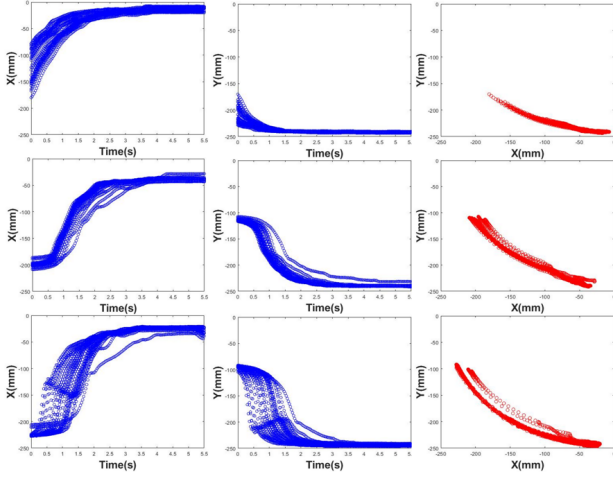
To assess actuator performance we evaluated the end-effector's: i) exerted force, ii) movement smoothness (using Spectral Arc length [SPARC] [30]), and iii) motion path length, as well as the maximum angle achieved at the shoulder joint during abduction/adduction.



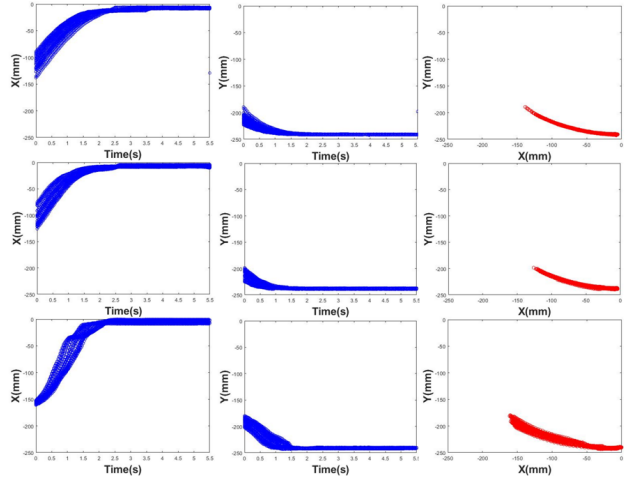
(a) Shoulder *abduction* during inflation of the **1-cell** actuator.



(c) Shoulder *abduction* during inflation of the **2-cell** actuator.



(b) Shoulder *adduction* during deflation of the **1-cell** actuator.



(d) Shoulder *adduction* during deflation of the **2-cell** actuator.

Fig. 5. Right arm's end-effector X and Y position, and the two-dimensional trajectories (curves in red) during abduction and adduction for the 1- and 2-cell actuators. Curves in the top, middle and bottom row correspond to 50%, 75% and 100% duty cycle, respectively.

B. Experimental Results and Discussion

To reach full inflation at $\{50, 75, 100\}\%$ duty cycle, it takes $\{4.5, 3.5, 2.7\}$ sec and $\{3.5, 2.5, 2\}$ sec on average for the 1-cell and 2-cell actuators, respectively. This suggests a roughly superlinear decrease of inflation time as PWM increases, for both actuators. Fig. 5 depicts the 2D position data of the end-effector during shoulder abduction and adduction for the 1-cell and 2-cell, respectively.

1) Force Generation: Forces exerted by the end-effector under 1-cell and 2-cell actuators are shown in Fig. 6. A two-way Analysis of Variance (ANOVA) was performed to identify differences in force profiles between the two types of actuators and across the different duty cycles. A statistically significant interaction between number of cells and % duty cycle was found ($F[2, 180] = 12.36, p = 0.000$) supporting that the number of cells has an effect on force generation at the 50% and 100% duty cycles but not at the 75%. In the aforementioned two duty cycles, the 1-cell actuator is the one that produces greater forces. Overall, force generation increases with increasing % duty cycle.

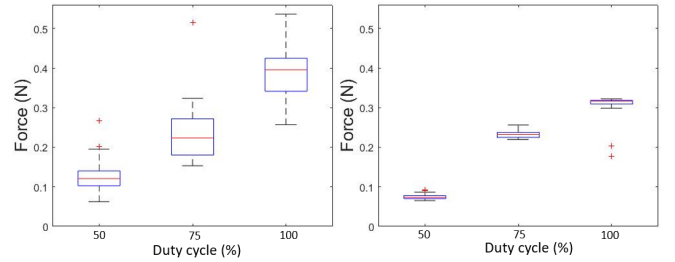


Fig. 6. The force exerted by the arm during full inflation for 1-cell (left) and 2-cell (right) shoulder actuators at 50%, 75% and 100% duty cycle.

2) Movement Smoothness: Two-way ANOVAs were performed to identify differences on smoothness across the two types of actuators and the different duty cycles, for each type of motion (abduction and adduction). For abduction, a significant interaction between number of cells and % duty cycle was found ($F[2, 539] = 37.50, p = 0.000$) supporting the % duty cycle affects differently the performance of the two actuators. For adduction, a significant difference only for the main effect of % duty cycle was found ($F[2, 539] = 85.08, p = 0.000$). Tukey post-hoc analysis showed that

smoothness is significantly less at the 50% duty cycle compared to the other two regardless of the number of cells ($p_{50\%-75\%} = 0.000$, $p_{50\%-100\%} = 0.000$, $p_{75\%-100\%} = 0.645$). Smoothness values along the axes (i.e. x, y and z) from IMU readings are shown in Table III.²

TABLE III
SMOOTHNESS (S) VALUES

Movement	Sample	Duty cycle	Smoothness (S)(Mean \pm SD)		
			S _x	S _y	S _z
Abduction	1 cell	50%	-7.67 \pm 1.99	-3.85 \pm 1.61	-2.4 \pm 0.50
		75%	-4.56 \pm 0.63	-5.34 \pm 0.84	-1.85 \pm 0.08
		100%	-3.27 \pm 0.76	-2.08 \pm 0.30	-1.97 \pm 0.07
	2 cell	50%	-4.48 \pm 0.54	-1.91 \pm 0.06	-1.85 \pm 0.70
		75%	-3.30 \pm 0.16	-1.90 \pm 0.11	-1.61 \pm 0.08
		100%	-4.64 \pm 0.81	-2.76 \pm 0.65	-1.88 \pm 0.06
Adduction	1 cell	50%	-5.30 \pm 0.86	-6.15 \pm 0.98	-2.7 \pm 0.21
		75%	-2.75 \pm 0.17	-4.20 \pm 2.00	-2.08 \pm 0.20
		100%	-3.54 \pm 0.45	-2.57 \pm 0.56	-1.91 \pm 0.04
	2 cell	50%	-6.70 \pm 0.62	-3.71 \pm 0.42	-2.37 \pm 0.17
		75%	-4.24 \pm 0.67	-2.23 \pm 0.23	-1.76 \pm 0.17
		100%	-3.75 \pm 1.15	-2.58 \pm 1.46	-2.11 \pm 0.21

3) *Path Length and Shoulder Angle*: Two-way ANOVAs were performed to identify differences on motion path length across the two types of actuators and the different duty cycles, for each type of motion (abduction and adduction). For abduction, a significant interaction between number of cells and duty cycles was found ($F[2,905] = 7.59$, $p = 0.001$) supporting that the % duty cycle affects differently the performance of the two actuators. Similarly, for adduction, a significant interaction between number of cells and duty cycles was found ($F[2,905] = 3.60$, $p = 0.028$) supporting that the % duty cycle affects differently the performance of the two actuators. Motion path profiles are depicted in Fig. 7.

As for the changes in angle at the shoulder joint, two observations can be pointed out. First, the range of motion on the vertical axis is greater with the 1-cell actuator compared to the 2-cell actuator. Second, the average maximum angle achieved with the 2-cell actuator at 100% duty cycle is similar to the average maximum angle achieved with the 1-cell actuator at 50% duty cycle, indicating that we can achieve higher elevation of the arm against gravity with the 1-cell actuator (Table IV).

Overall, the aforementioned findings inform next steps into the design and control (more information in [32]) of our wearable device as well as considerations for its use. For example, although the 1-cell actuator achieves greater elevation of the arm and generates greater forces, comes with limitations that can be addressed with the 2-cell actuator. Fig. 5 and TableV present visual and quantitative (Coefficient of Variation [CV]) data that support a greater trial-to-trial variation in force generation and end-effector x,y position across every % duty cycle for the 1-cell actuator that is not observed with the 2-cell actuator. In addition, as the 1-cell

² We used the continuous data streams of gyroscopic data collected in the IMU on a SPARC-based approach to quantitatively measure the movement smoothness [30], [31]. The adaptive cut-off frequency was determined to be 5 Hz from the signal power spectral density. The signals were low-pass filtered with a zero-lag second order Butterworth filter with a cut-off frequency at 5 Hz to remove the high-frequency noise.

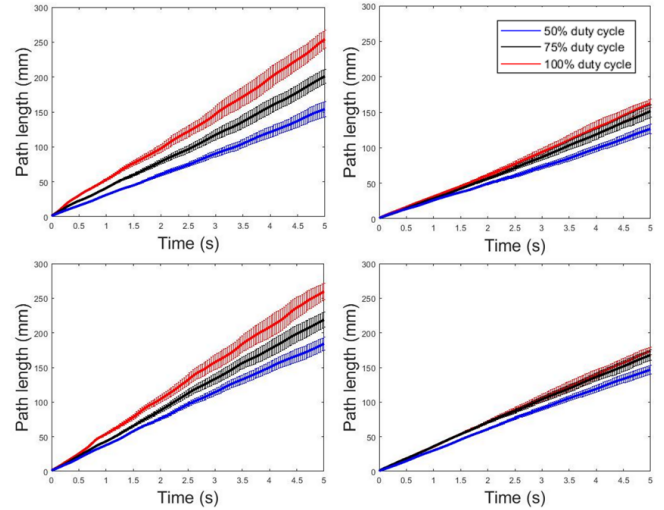


Fig. 7. Motion path length of end-effector with 1-cell (left) and 2-cell (right) actuators at inflation (top) and deflation (bottom) across duty cycles.

TABLE IV
SHOULDER ANGLE

Actuator	Duty cycle	Shoulder Angle (degree) (Mean \pm SD)
1 cell	50%	41.92 \pm 1.84
	75%	53.40 \pm 1.06
	100%	63.89 \pm 1.91
2 cell	50%	34.43 \pm 0.66
	75%	39.87 \pm 0.36
	100%	41.89 \pm 0.50

TABLE V
COEFFICIENT OF VARIATION(CV)

Actuator	Duty cycle	Force	Smoothness	Path length
1 cell	50%	0.33	0.58	0.59
	75%	0.30	0.46	0.58
	100%	0.18	0.30	0.57
2 cell	50%	0.09	0.50	0.59
	75%	0.04	0.40	0.59
	100%	0.11	0.44	0.58

actuator achieves full inflation and leads to maximum joint angle, it protrudes from the underarm placement. The 2-cell actuator, on the other hand, remains in place throughout the inflation making it more low-profile for our wearable (Fig. 8).

IV. CONCLUSION AND FUTURE WORK

This paper demonstrates the design and evaluation of a family of new fabric-based actuators for the infant shoulder. Among 20 initially-proposed multi-cell designs first evaluated in simulation, two actuators (1-cell and 2-cell) were down-selected and tested on a physical infant-sized model. Overall, the 1-cell actuator seems to generate forces and arm motion that are appropriate for our application; nevertheless, trial-to-trial variation is less for the 2-cell actuator indicating a higher reproducibility. Although fabric-based actuators may come with limitations such as low force generation [33], for our purpose (i.e. use with infants), we found these forces adequate to lift the arms against gravity. Future work will



Fig. 8. The actuators in deflated (top) and inflated (bottom) states. From left to right: 1-cell, 2-cell, and 1-cell actuator placed within a detachable double-layered pocket. Box in red indicates the housing space of the actuator in the pocket. The hook on the pocket connects with the loop on the wearable.

focus on supporting other UE joints, developing closed-loop controllers [32], and eventually testing with infants.

REFERENCES

- [1] M. A. Lobo, J. C. Galloway, and J. C. Heathcock, "Characterization and intervention for upper extremity exploration & reaching behaviors in infancy," *Journal of Hand Therapy*, vol. 28, no. 2, pp. 114–125, 2015.
- [2] S. Henderson, H. Skelton, and P. Rosenbaum, "Assistive devices for children with functional impairments: impact on child and caregiver function," *Developmental Medicine & Child Neurology*, vol. 50, no. 2, pp. 89–98, 2008.
- [3] A. J. Arnold, J. L. Haworth, V. O. Moran, A. Abulhasan, N. Steinbuch, and E. Kokkoni, "Exploring the Unmet Need for Technology to Promote Motor Ability in Children Younger Than 5 Years of Age: A Systematic Review," *Archives of Rehabilitation Research and Clinical Translation*, vol. 2, no. 2, p. 100051, 2020.
- [4] I. Babik, E. Kokkoni, A. B. Cunha, J. C. Galloway, T. Rahman, and M. A. Lobo, "Feasibility and effectiveness of a novel exoskeleton for an infant with arm movement impairments," *Pediatric Physical Therapy*, vol. 28, no. 3, p. 338, 2016.
- [5] M. A. Lobo, J. Koshy, M. L. Hall, O. Erol, H. Cao, J. M. Buckley, J. C. Galloway, and J. Higginson, "Playskin lift: Development and initial testing of an exoskeletal garment to assist upper extremity mobility and function," *Physical Therapy*, vol. 96, pp. 390–399, 3 2016.
- [6] T. G. Sugar, J. He, E. J. Koeneman, J. B. Koeneman, R. Herman, H. Huang, R. S. Schultz, D. Herring, J. Wanberg, S. Balasubramanian *et al.*, "Design and control of Rupert: a device for robotic upper extremity repetitive therapy," *IEEE transactions on neural systems and rehabilitation engineering*, vol. 15, no. 3, pp. 336–346, 2007.
- [7] E. Kokkoni, Z. Liu, and K. Karydis, "Development of a soft robotic wearable device to assist infant reaching," *Journal of Engineering and Science in Medical Diagnostics and Therapy*, vol. 3, no. 2, 2020.
- [8] P. Polygerinos, S. Lyne, Z. Wang, L. F. Nicolini, B. Mosadegh, G. M. Whitesides, and C. J. Walsh, "Towards a soft pneumatic glove for hand rehabilitation," in *IEEE/RSJ International Conference on Intelligent Robots and Systems*, 2013, pp. 1512–1517.
- [9] P. Maeder-York, T. Clites, E. Boggs, R. Neff, P. Polygerinos, D. Holland, L. Stirling, K. Galloway, C. Wee, and C. Walsh, "Biologically Inspired Soft Robot for Thumb Rehabilitation," *Journal of Medical Devices*, vol. 8, no. 2, 04 2014.
- [10] P. Polygerinos, K. C. Galloway, S. Sanan, M. Herman, and C. J. Walsh, "Emg controlled soft robotic glove for assistance during activities of daily living," in *IEEE International Conference on Rehabilitation Robotics (ICORR)*, 2015, pp. 55–60.
- [11] Y.-L. Park, B.-r. Chen, N. O. Pérez-Arancibia, D. Young, L. Stirling, R. J. Wood, E. C. Goldfield, and R. Nagpal, "Design and control of a bio-inspired soft wearable robotic device for ankle-foot rehabilitation," *Bioinspiration & Biomimetics*, vol. 9, no. 1, p. 016007, 2014.
- [12] H. K. Yap, P. M. Khin, T. H. Koh, Y. Sun, X. Liang, J. H. Lim, and C.-H. Yeow, "A fully fabric-based bidirectional soft robotic glove for assistance and rehabilitation of hand impaired patients," *IEEE Robotics and Automation Letters*, vol. 2, no. 3, pp. 1383–1390, 2017.
- [13] P. H. Nguyen, C. Sparks, S. G. Nuthi, N. M. Vale, and P. Polygerinos, "Soft poly-limbs: Toward a new paradigm of mobile manipulation for daily living tasks," *Soft Robotics*, vol. 6, no. 1, pp. 38–53, 2019.
- [14] S. Kim, C. Laschi, and B. Trimmer, "Soft robotics: a bioinspired evolution in robotics," *Trends in Biotechnology*, vol. 31, no. 5, pp. 287–294, 2013.
- [15] F. Iida and C. Laschi, "Soft robotics: Challenges and perspectives," *Procedia Computer Science*, vol. 7, pp. 99–102, 2011.
- [16] G. Agarwal, N. Besuchet, B. Audergon, and J. Paik, "Stretchable materials for robust soft actuators towards assistive wearable devices," *Scientific Reports*, vol. 6, no. 1, pp. 1–8, 2016.
- [17] C. Majidi, "Soft robotics: A perspective - current trends and prospects for the future," *Soft Robotics*, vol. 1, pp. 5–11, 2014.
- [18] H. Xiong and X. Diao, "A review of cable-driven rehabilitation devices," *Disability and Rehabilitation: Assistive Technology*, vol. 15, no. 8, pp. 885–897, 2020.
- [19] B. Gorissen, D. Reynaerts, S. Konishi, K. Yoshida, J.-W. Kim, and M. De Volder, "Elastic inflatable actuators for soft robotic applications," *Advanced Materials*, vol. 29, no. 43, p. 1604977, 2017.
- [20] Y. Yang, Y. Chen, Y. Li, M. Z. Chen, and Y. Wei, "Bioinspired robotic fingers based on pneumatic actuator and 3d printing of smart material," *Soft Robotics*, vol. 4, no. 2, pp. 147–162, 2017.
- [21] J. H. Low, N. Cheng, P. Khin, N. V. Thakor, S. L. Kukreja, H. Ren, and C.-H. Yeow, "A bidirectional soft pneumatic fabric-based actuator for grasping applications," in *IEEE/RSJ International Conference on Intelligent Robots and Systems (IROS)*, 2017, pp. 1180–1186.
- [22] S. Sanan, P. S. Lynn, and S. T. Griffith, "Pneumatic torsional actuators for inflatable robots," *Journal of Mechanisms and Robotics*, vol. 6, no. 3, p. 031003, 2014.
- [23] C. M. Best, J. P. Wilson, and M. D. Killpack, "Control of a pneumatically actuated, fully inflatable, fabric-based, humanoid robot," in *IEEE-RAS International Conference on Humanoid Robots (Humanoids)*, 2015, pp. 1133–1140.
- [24] J. Park, J. Choi, S. J. Kim, K.-H. Seo, and J. Kim, "Design of an inflatable wrinkle actuator with fast inflation/deflation responses for wearable suits," *IEEE Robotics and Automation Letters*, vol. 5, no. 3, pp. 3799–3805, 2020.
- [25] C. S. Simpson, A. M. Okamura, and E. W. Hawkes, "Exomuscle: An inflatable device for shoulder abduction support," in *IEEE International Conference on Robotics and Automation (ICRA)*, 2017, pp. 6651–6657.
- [26] C. Simpson, B. Huerta, S. Sketch, M. Lansberg, E. Hawkes, and A. Okamura, "Upper extremity exomuscle for shoulder abduction support," *IEEE Transactions on Medical Robotics and Bionics*, vol. 2, no. 3, pp. 474–484, 2020.
- [27] B. Li, B. Greenspan, T. Mascitelli, M. Raccuglia, K. Denner, R. Duda, and M. A. Lobo, "Design of the Playskin Air(TM): A User-Controlled, Soft Pneumatic Exoskeleton," in *Proceedings of the 2019 Design of Medical Devices Conference*, 2019, pp. 1–4.
- [28] D. Paez-Granados, T. Yamamoto, H. Kadone, and K. Suzuki, "Passive flow control for series inflatable actuators: Application on a wearable soft-robot for posture assistance," *IEEE Robotics and Automation Letters*, vol. 6, no. 3, pp. 4891–4898, 2021.
- [29] C. D. Fryar, M. D. Carroll, Q. Gu, J. Afful, and C. L. Ogden, "Anthropometric reference data for children and adults: United states, 2015-2018," 2021.
- [30] A. Melendez-Calderon, C. Shirota, and S. Balasubramanian, "Estimating movement smoothness from inertial measurement units," *Frontiers in Bioengineering and Biotechnology*, p. 1507, 2021.
- [31] Y. Beck, T. Herman, M. Brozgol, N. Giladi, A. Mirelman, and J. M. Hausdorff, "Sparc: a new approach to quantifying gait smoothness in patients with parkinson's disease," *Journal of Neuroengineering and Rehabilitation*, vol. 15, no. 1, pp. 1–9, 2018.
- [32] C. Mucchiani, Z. Liu, I. Sahin, J. Dube, L. Vu, E. Kokkoni, and K. Karydis, "Closed-loop position control of a pediatric soft robotic wearable device for upper extremity assistance," in *IEEE International Conference on Robot & Human Interactive Communication (RO-MAN)*, 2022.
- [33] G. Belforte, G. Eula, A. Ivanov, and S. Siroli, "Soft pneumatic actuators for rehabilitation," in *Actuators*, vol. 3, no. 2. MDPI, 2014, pp. 84–106.